



Cite this: *Soft Matter*, 2016, **12**, 9575

Dielectric effects on the ion distribution near a Janus colloid

Huanxin Wu,^a Ming Han^b and Erik Lijten^{*acd}

Spherical Janus colloids, particles with different surface properties on their two hemispheres, are generally heterogeneous in permittivity. This dielectric heterogeneity may affect their behavior in electrolytes and external electric fields, but is typically not taken into account in computational studies. We apply the iterative dielectric solver developed by Barros and Lijten [*Phys. Rev. Lett.*, 2014, **113**, 017801] in combination with preconditioning techniques that can accurately and efficiently compute the polarization of dielectrically anisotropic particles. Employing this approach, we systematically study the ion distribution around neutral and charged Janus particles with various permittivities, immersed in symmetric and asymmetric electrolytes. We demonstrate that neutral Janus colloids may carry a nonzero dipole moment in asymmetric salts. For charged Janus colloids, dielectric effects can substantially influence the electric double layer. These findings also have implications for other dielectrically anisotropic entities, such as proteins.

Received 22nd July 2016,
Accepted 18th October 2016

DOI: 10.1039/c6sm01675h

www.rsc.org/softmatter

1 Introduction

The long-range nature of electrostatic interactions contributes to many properties of colloidal dispersions,^{1–4} and must be taken into account in computer simulations. For dielectrically homogeneous systems, fast Ewald solvers are in wide-spread use. However, many phenomena of interest occur at colloidal interfaces, where the dielectric mismatch between the solvent and the colloid gives rise to induced surface (polarization) charge, which is analytically complicated and computationally expensive to solve. Whereas current experimental techniques face limitations in measuring these interfacial properties at a molecular level, computer simulations can offer much insight. For isotropic colloids, the polarization effects on the ionic density profile near colloidal surfaces are well-studied *via* simulations and have been shown to be significant.^{5–8} Such effects on the structure of the electric double layer (EDL) surrounding a colloid may have consequences for many properties, such as surface ionization and complexation, chemical reactions, and electrophoretic mobility.⁹

Recently, particles with anisotropic surface properties have attracted strong interest due to their promise for applications in photonic materials, electronics, electrokinetics, and drug delivery.¹⁰

One of the simplest patchy geometries is the Janus particle, which comprises two domains of different materials.^{11,12} There are many possible design choices for the mismatch between these domains,¹³ including dipolar,^{14,15} charged/hydrophobic,^{16,17} or charged/magnetic,¹⁸ resulting in a variety of self-assembled structures.^{15,16,18,19} Current large-scale fabrication techniques can produce Janus particles with controllable sizes and geometries.¹¹ One of the methodologies for creating spherical Janus colloids is the application of a partial coating of a different material on a spherical colloid. The resulting dielectric heterogeneity in the particle is crucial for a variety of phenomena, including the well-known induced-charge electrophoresis.²⁰ Yet, owing to a lack of efficient modeling methods, most computer simulation studies ignore the polarization of Janus particles by the electrolyte.^{15,21–24}

For complicated geometries like Janus particles, boundary-element method (BEM)-based dielectric solvers offer advantages in convenience, capability, and efficiency.²⁵ Instead of solving Poisson's equation on a three-dimensional grid, the BEM only discretizes dielectric interfaces and solves the surface induced charge explicitly. Here, we apply the approach introduced in ref. 26 and 27 to investigate the ionic distribution around a Janus colloid *via* molecular dynamics simulations, in which the induced charges at dielectric interfaces are computed dynamically. We also adopt preconditioning techniques that can significantly improve the accuracy and efficiency for systems with multiple dielectric contrasts.²⁸ This method has been successfully applied to study the EDL of anisotropic dielectric colloids under external electric fields.²⁹

This paper is organized as follows. First, key concepts of the BEM-based iterative dielectric solver (IDS) are reviewed in

^a Department of Physics and Astronomy, Northwestern University, Evanston, Illinois 60208, USA

^b Graduate Program in Applied Physics, Northwestern University, Evanston, Illinois 60208, USA

^c Department of Materials Science and Engineering Northwestern University, Evanston, Illinois 60208, USA. E-mail: lijten@northwestern.edu

^d Department of Engineering Sciences and Applied Mathematics, Northwestern University, Evanston, Illinois 60208, USA

Section 2.1. Details of our simulation model are provided in Section 2.2. After examining the effects of Janus particle coating thickness in Section 2.3 we proceed to apply the IDS to examine the structure of symmetric and asymmetric electrolytes near two types of neutral Janus colloids (silica/silicon and silica/metal) in Section 3.1. Following that, Section 3.2 presents simulation results for the counterion distribution around various charged Janus colloids in both salt-free and electrolyte environments. We address the effects of colloid size and ion radius in Section 3.3. We conclude the paper with a brief summary in Section 4.

2 Methods and model

2.1 Iterative dielectric solver

We model a Janus colloid immersed in electrolyte using the primitive model, which treats the Janus colloid and the ions as finite-size particles but the background solvent as a (uniform) dielectric continuum. The Janus colloid consists of piecewise uniform dielectric domains. On the opposing sides of an arbitrary interface location \mathbf{s} , we have different relative permittivities $\varepsilon_{\text{in}}(\mathbf{s})$ and $\varepsilon_{\text{out}}(\mathbf{s})$ with outward unit normal $\hat{\mathbf{n}}(\mathbf{s})$. Without loss of generality, we assume free charge distributions $\sigma_f(\mathbf{s})$ on the interfaces and $\rho_f(\mathbf{r})$ in the bulk, both of which induce a surface polarization charge density $\sigma_{\text{pol}}(\mathbf{s})$. In the bulk, polarization charges only exist at free charge locations with density $\rho_f(\mathbf{r})[1/\varepsilon(\mathbf{r}) - 1]$. As this can be accounted for in a straightforward manner, our efforts focus on dynamically solving the surface polarization charge density $\sigma_{\text{pol}}(\mathbf{s})$. The technical aspects of the induced-charge calculation are somewhat intricate; here, we only provide a concise overview. For a detailed description we refer to the original methods publication²⁶ and to a comparison with calculations based upon image charges.²⁵

Instead of solving the conventional Poisson equation, BEM-based dielectric solvers aim to solve integral forms of Poisson's equation that are more suited for finding boundary values (such as $\sigma_{\text{pol}}(\mathbf{s})$ in the situation considered here) rather than the electrostatic potential throughout the space. The iterative dielectric solver introduced in ref. 26 utilizes the following integral equation (for a detailed derivation, see eqn (36) therein),

$$\bar{\varepsilon}(\mathbf{s})[\sigma_f(\mathbf{s}) + \sigma_{\text{pol}}(\mathbf{s})] + \varepsilon_0 \Delta \varepsilon(\mathbf{s}) \hat{\mathbf{n}}(\mathbf{s}) \cdot \mathbf{E}(\mathbf{s}) = \sigma_f(\mathbf{s}), \quad (1)$$

where $\bar{\varepsilon}(\mathbf{s}) = [\varepsilon_{\text{in}}(\mathbf{s}) + \varepsilon_{\text{out}}(\mathbf{s})]/2$, $\Delta \varepsilon(\mathbf{s}) = \varepsilon_{\text{out}}(\mathbf{s}) - \varepsilon_{\text{in}}(\mathbf{s})$, and ε_0 is the vacuum permittivity. The electric field $\mathbf{E}(\mathbf{s})$ arises from all free and induced charges in the system \mathbf{V} , including the surfaces \mathbf{S} and the bulk $\mathbf{V} \setminus \mathbf{S}$,

$$\begin{aligned} \mathbf{E}(\mathbf{s}) = & \lim_{\delta \rightarrow 0} \iint_{\mathbf{S}, |\mathbf{s} - \mathbf{s}'| > \delta} \frac{[\sigma_f(\mathbf{s}') + \sigma_{\text{pol}}(\mathbf{s}')](\mathbf{s} - \mathbf{s}')}{4\pi\varepsilon_0 |\mathbf{s} - \mathbf{s}'|^3} d\mathbf{s}' \\ & + \iint_{\mathbf{V} \setminus \mathbf{S}} \frac{\rho_f(\mathbf{r}')(\mathbf{s} - \mathbf{r}')}{4\pi\varepsilon_0 \varepsilon(\mathbf{r}') |\mathbf{s} - \mathbf{r}'|^3} d\mathbf{r}', \end{aligned} \quad (2)$$

where, to avoid the divergence of the layer potential, the infinitesimal disk $|\mathbf{s} - \mathbf{s}'| \leq \delta$ is excluded. $\varepsilon(\mathbf{r}')$ is the relative permittivity at the off-surface location \mathbf{r}' .

Eqn (1), a Fredholm integral equation of the second kind, can only be solved analytically for very simple geometries. The BEM

seeks the solution numerically *via* surface discretization. If we assume a constant surface charge density across a surface patch, use the patch centers to evaluate the integrals in eqn (2) *via* one-point quadrature, and employ discrete charge distributions in the bulk, eqn (1) can be rewritten as a self-consistent matrix equation $\mathcal{A}\sigma = \mathbf{b}$, with

$$\mathcal{A}_{ij} = \bar{\varepsilon}_i \delta_{ij} + a_j \frac{\Delta \varepsilon_i \hat{\mathbf{n}}_i \cdot (\mathbf{s}_i - \mathbf{s}_j)}{4\pi |\mathbf{s}_i - \mathbf{s}_j|^3}, \quad (3)$$

$$b_i = -\frac{\Delta \varepsilon_i}{4\pi} \sum_k \frac{q_k}{\varepsilon(\mathbf{r}_k)} \frac{\hat{\mathbf{n}}_i \cdot (\mathbf{s}_i - \mathbf{r}_k)}{|\mathbf{s}_i - \mathbf{r}_k|^3} + \sigma_f(\mathbf{s}_i), \quad (4)$$

where $\sigma(\mathbf{s}_i) = \sigma_{\text{pol}}(\mathbf{s}_i) + \sigma_f(\mathbf{s}_i)$, a_j is the area of the j th patch, and q_k is the charge of the k th ion in the bulk. Note that this implies that the target variable has been changed from the surface polarization charge density to the total surface charge density. As the free surface charges are fixed and known, this is a mathematically straightforward step, but it simplifies evaluation of the Coulomb interaction evaluation between patches.

For N surface patches, the matrix equation can be solved *via* matrix inversion, at a computational cost $\mathcal{O}(N^3)$. Instead, we solve it iteratively. Each iteration requires a matrix-vector multiplication which conventionally takes $\mathcal{O}(N^2)$ operations. However, since our particular operator \mathcal{A}_{ij} effectively computes pairwise Coulomb interactions, this can be accelerated *via* a fast Ewald solver. Thus, the computational cost of the IDS has the same scaling with the number of charges as the fast Ewald solver employed. For the particle-particle particle-mesh (PPPM) Ewald solver used in this paper, we achieved a scaling of $\mathcal{O}((N + M) \log(N + M))$, if the system contains M free point charges in addition to the N surface patches. Beyond this scaling advantage, iterative methods with fast Ewald solvers also include the periodic images automatically, which is crucial for many simulations. To optimize the convergence rate, we apply the Generalized Minimal Residual method (GMRES)³⁰ (see Section V.A in ref. 26 for a discussion of alternative solvers). Lastly, the efficiency and accuracy of the matrix solver are highly dependent on the matrix condition number. As demonstrated in ref. 28, to improve the accuracy and further increase the convergence rate it is essential to enforce the total induced charge on the Janus colloid to be zero and to apply Jacobi preconditioning to the matrix equation to avoid ill-conditioning of the matrix \mathcal{A} , arising from the presence of multiple distinct dielectric mismatches.

Once the surface induced charge density is obtained, electrostatic forces can be directly evaluated for molecular dynamics (MD) simulations without performing energy derivatives.

2.2 Molecular dynamics simulation model

To study dielectric effects on the EDL, we investigate a single dielectric Janus colloid of valence Z immersed in an aqueous electrolyte. The Janus sphere is comprised of two hemispheres of different materials and exhibits three dielectric interfaces: two hemispherical surfaces and one equatorial disk (Fig. 1). The particle has azimuthal symmetry about the z -axis. We consider

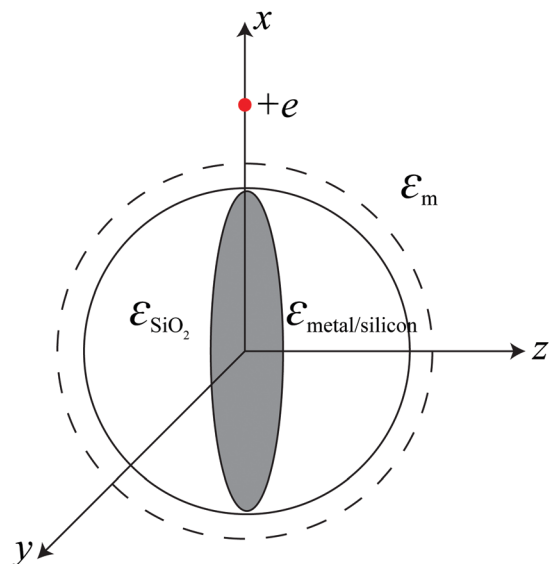


Fig. 1 A silica/metal/silicon Janus particle (solid circle) comprised of two hemispheres that are separated by a disk-shaped dielectric interface (shaded region). To ensure that mobile external charges (ions) do not approach the particle surface—i.e., the dielectric interface separating the hemispheres from the surrounding medium—too closely, it is surrounded by a concentric spherical surface (dashed circle). This outer surface is modeled *via* a soft repulsive potential (*cf.* main text). The dielectric sphere has a diameter 14σ (with $\sigma = 7.14$ Å), whereas the effective diameter of the particle is 15σ (i.e., the dielectric interface is located 0.5σ below the effective particle surface). As a test case for the effects of coating thickness (Section 2.3), we examine the surface potential induced by a positive unit charge located at $(9\sigma, 0, 0)$.

two representative types of dielectrically heterogeneous Janus colloids. The first type consists of hemispheres made of silica ($\epsilon_{\text{SiO}_2} = 4$) and silicon ($\epsilon_{\text{Si}} = 12$), respectively. The second type has a silica hemisphere and a metal hemisphere, where the conducting side is approximated by a high permittivity $\epsilon_{\text{h}} = 10^5$. The system is embedded in water ($\epsilon_{\text{m}} = 80$). The spherical BEM mesh, *i.e.*, the dielectric interface between the water and the particle, has a radius $R = 7\sigma$, where $\sigma = 7.14$ Å is the Bjerrum length of water at room temperature. To prevent the ions from penetrating the BEM mesh, this dielectric interface is placed inside a concentric soft repulsive shell, modeled by a shifted-truncated Lennard-Jones (LJ) potential described below. As a result, the Janus particle has an effective diameter $d = 15\sigma = 10.71$ nm. As this is far smaller than the particle sizes typically employed in experiment, we systematically examine the effect of colloid size on our results in Section 3.3. Since the Janus particle is much larger than the ions, we only discretize the dielectric interfaces of the Janus particle, *i.e.*, we ignore anisotropic polarization charge distribution on the hydrated ions.³¹ This approximation implies that we also ignore the corresponding charge–dipole and dipole–dipole interactions between ions, as well as dielectrophoretic forces. Another simplification concerns the permittivity of the electrolyte solution, which is known to decrease with increasing ion concentration.³² Capturing this effect requires solving the spatial and time-dependent bulk polarization, which goes beyond the assumption of sharp dielectric interfaces adopted here, but will be addressed in future work.

For the BEM mesh, the central disk is discretized into 183 patches and the spherical dielectric interface into 732 patches. These 732 patches are then assigned to either hemisphere, depending on the position of their center. Owing to our choice for the orientation of the mesh, this results in 363 and 369 patches belonging to either side, respectively. The Janus colloid is fixed at the center of a periodic cubic simulation box ($30 \times 30 \times 30\sigma^3$), and is surrounded by hydrated ions that are represented as spheres of diameter σ . For the systems investigated, the Debye length is smaller than $1/10$ of the simulation box size, so that artifacts due to periodic images are negligible.

The electrostatic interactions are taken into account *via* PPPM Ewald summation, with a relative accuracy of 10^{-4} .^{33,34} Excluded-volume interactions between particles i and j are modeled *via* an expanded shifted-truncated Lennard-Jones (LJ) potential,

$$u_{\text{LJ}}(r_{ij}) = \begin{cases} \infty & r_{ij} \leq \Delta_{ij} \\ 4k_{\text{B}}T \left[\left(\frac{\sigma}{r_{ij} - \Delta_{ij}} \right)^{12} - \left(\frac{\sigma}{r_{ij} - \Delta_{ij}} \right)^6 + \frac{1}{4} \right] & \Delta_{ij} < r_{ij} < \Delta_{ij} + 2\frac{1}{6}\sigma, \\ 0 & r_{ij} \geq \Delta_{ij} + 2\frac{1}{6}\sigma \end{cases} \quad (5)$$

where $\Delta_{ij} = (d_i + d_j)/2 - \sigma$ is the hard-core distance, with d_i and d_j the diameters of particles i and j . Whereas this potential diverges at $r_{ij} = \Delta_{ij}$, the repulsive interaction already equals the thermal energy at $r_{ij} = \Delta_{ij} + \sigma = (d_i + d_j)/2$. According to ref. 26, the average patch–patch separation must be chosen smaller than the minimum ion–patch distance, to suppress discretization effects. In our system, the closest ion–colloid separation is $r = 8\sigma$, which allows a surface discretization with an average patch–patch separation of approximately σ .

To investigate the EDL structure, we perform MD simulations of the ions surrounding the colloid. Depending on the system configuration, 232 to 867 ions are involved. To introduce thermal fluctuations, a Langevin thermostat is applied to the ions, with damping parameter $20t_0$, where $t_0 = (m\sigma^2/k_{\text{B}}T)^{1/2}$ is the LJ unit time with m the ionic mass, to keep the system at room temperature ($T = 298$ K). The resultant Bjerrum length $l_{\text{B}} = e^2/(4\pi\epsilon_0\epsilon_{\text{m}}k_{\text{B}}T) = \sigma = 7.14$ Å coincides with the ion size. Each simulation starts from a random ion configuration. After an equilibration period of $2500 t_0$, we sample the ion distribution over 150 000 time steps with 200 to 600 independent runs for each parameter set, which yields 2×10^5 to 6×10^5 independent samples.

2.3 Effects of coating thickness

In many experiments, dielectrically anisotropic Janus colloids are created by deposition of a thin metal coating,^{18,20} as opposed to the evenly divided model of Fig. 1. To confirm that our model properly captures the polarization effects of a Janus particle generated by coating, we examine the effects of coating thickness of a silica/metal Janus particle *via* finite-element calculation using COMSOL (Version 5.1, 2015), a commercial finite-element code. Under the same system setup as described in

the previous section (*i.e.*, Janus director oriented along the z axis), in the absence of electrolyte, we place a positive external point charge in the equatorial plane and $\delta = 2\sigma$ away from the dielectric interface (Fig. 1). We consider a silica sphere with one hemisphere coated by metal. The coating thickness is parametrized by its ratio t with respect to the (dielectric) radius $R = 7\sigma$. To ensure high accuracy and a smooth surface potential, we mesh the system with more than 3×10^6 tetrahedral elements. As illustrated in Fig. 2, the surface potential depends strongly on thickness only for very thin coatings, starting to saturate already at $t \sim 0.01$ —thinner than the coating applied in most experiments. Thus, to a good approximation, we can model the Janus colloids as evenly divided spheres, with results that also represent the dielectric response of Janus particles with surface coatings.

The surface potential shown in Fig. 2 is the sum of the source potential of the unit charge and the image potential induced by this charge. Whereas the charge is equidistant to both hemispheres, their dielectric response is very different. It is also informative to compare the surface potential to the image potential, shown in Fig. 3, solely arising from the induced electric charges on the colloidal surface. It illustrates, *e.g.*, how the constant surface potential on the metal hemisphere (Fig. 2, for $t \geq 0.01$) arises from the image potential that varies with the polar angle and from the equally varying source potential.

3 Results

3.1 Electrolyte near a neutral dielectric Janus colloid

We first consider a neutral Janus dielectric colloid ($Z = 0$, no counterions) embedded in an aqueous electrolyte. Here, all

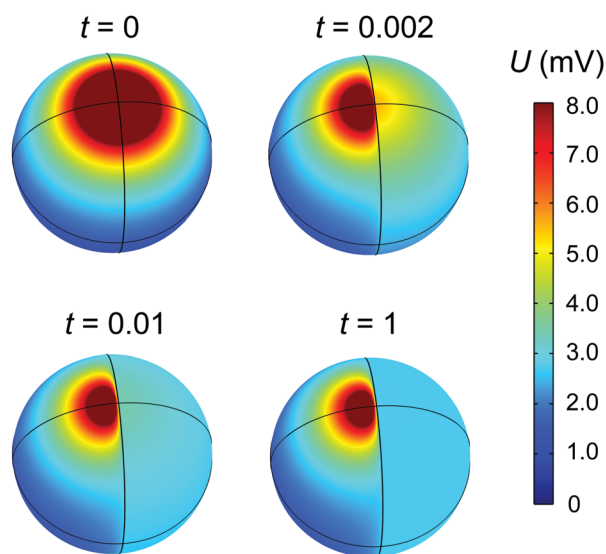


Fig. 2 Surface potential of a silica (left)/metal (right) Janus sphere induced by an external unit charge, for four different thicknesses of the metal coating: $t = 0$ (a pure silica sphere), 0.002, 0.01, and 1 (evenly divided Janus sphere), where t is the ratio between coating thickness and particle radius. The orientation of the Janus particle and the location of the charge are the same as in Fig. 1. Although the potential is thickness dependent, it has nearly saturated for a thickness of 1% ($t = 0.01$). The potential on the right-hand side of the colloid becomes uniform, as expected for a metal.

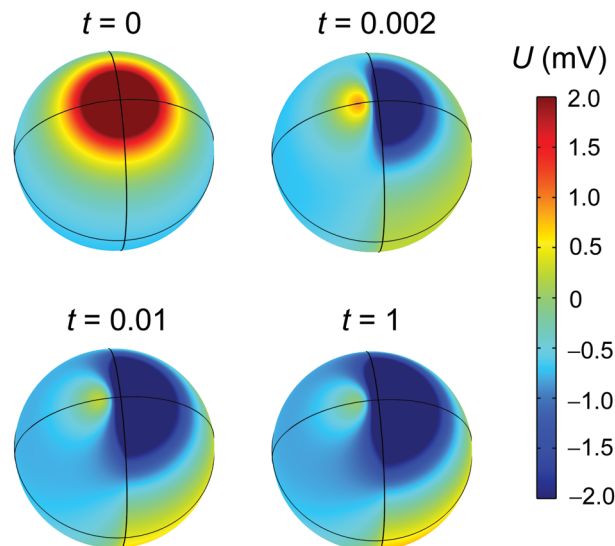


Fig. 3 Image potential of the same system as depicted in Fig. 2, *i.e.*, a silica (left)/metal (right) Janus sphere and an external unit charge, with 4 different metal coating thicknesses. The potential shown here is solely due to the electric charges induced on the colloidal surface.

electrostatic interactions between the Janus colloid and the ions are purely due to polarization charges induced on the colloid. This allows us to isolate the dielectric response and compare the double layer around Janus colloids with different dielectric contrasts. We note that an ion of valence z located on the lower permittivity side of a dielectric interface induces an attractive polarization charge proportional to z , and *vice versa*. Thus, the dielectric interaction is proportional to z^2 .

3.1.1 Symmetric monovalent salt. For the silica/silicon Janus colloid, dielectric effects are repulsive for both hemispheres, since $\epsilon_{\text{SiO}_2} < \epsilon_{\text{Si}} < \epsilon_{\text{m}}$. As the system exhibits azimuthal symmetry around the z -axis (Fig. 1), we calculate the ionic density distribution $c(r, \theta)$. As illustrated in Fig. 4, we indeed observe a very weak depletion region near both hemispheres beyond $r_c = 8.12\sigma$ (dashed vertical line), where the LJ interactions vanish, due to dielectric repulsion. Even though the two hemispheres differ by a factor 3 in dielectric mismatch ($\epsilon_{\text{Si}} = 3\epsilon_{\text{SiO}_2}$), no clear dependence on the polar angle θ is observed. Thus, in this case the Janus colloid behaves similar to an isotropic colloid, simply because the dielectric contrast with the surrounding medium $\Delta\epsilon/\bar{\epsilon}$ (*cf.* eqn (1)) differs only by 20% for the two materials.

The situation becomes more interesting when the two hemispheres have opposite dielectric responses. For a silica/metal Janus colloid, the silica side is repulsive to ions whereas the metal side is attractive. This is reflected in the ionic density distribution (Fig. 5), with a notable accumulation of ions near the metal hemisphere. The interference between the metal and the silica hemispheres is very small, as $c(r, \theta)$ on the silica side is indistinguishable from that in Fig. 4. An interesting consequence of the anisotropic ion distribution is the presence of a net entropic force of strength $(-0.87 \pm 0.03k_{\text{B}}T/l_{\text{B}})$, oriented along the symmetry axis (director) of the silica/metal Janus particle and pointing towards the silica side. Energy conservation

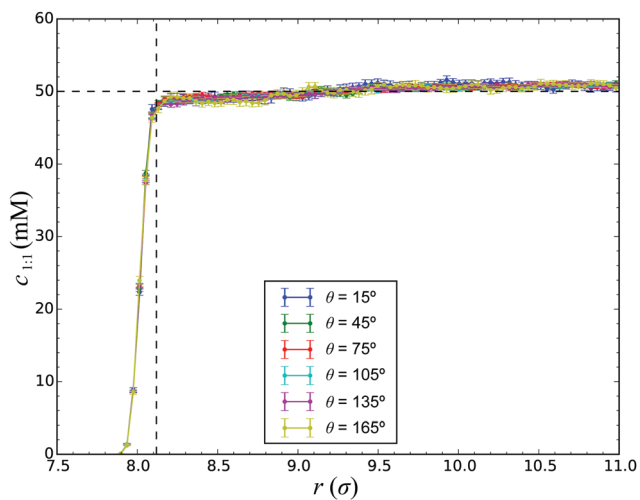


Fig. 4 Ionic density distribution $c(r, \theta)$ of 50 mM monovalent aqueous salt around a silica/silicon Janus colloid at various θ , where θ is the polar angle with respect to the symmetry axis of the Janus colloid, *i.e.*, $0 \leq \theta < 90^\circ$ refers to the silicon hemisphere and $90^\circ < \theta \leq 180^\circ$ to the silica hemisphere. For each θ , the ion concentration is averaged over $[\theta - 1.5^\circ, \theta + 1.5^\circ]$. The dashed horizontal line marks the bulk concentration and the dashed vertical line marks the LJ interaction cutoff distance. Whereas the relative permittivities of both materials differ by a factor 3, their dielectric contrast with the surrounding medium is comparable, so that the ion distribution shows no θ dependence.

requires that this force, arising from the imbalanced (purely repulsive) excluded-volume LJ interactions between ions and the colloidal surface, be counteracted by other interactions. Indeed, we find that the electrostatic interactions between the ions and the induced surface charge give rise to a net electrostatic force ($0.8971 \pm 0.0007 k_B T/l_B$), directed towards the metal side.

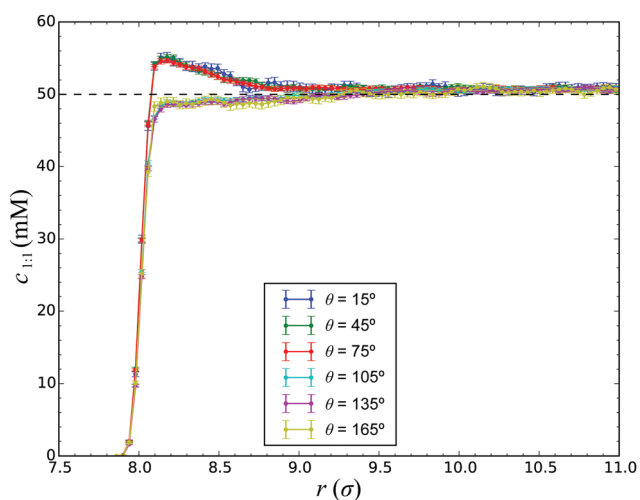


Fig. 5 Ionic density distribution $c(r, \theta)$ of 50 mM monovalent salt around a single silica/metal Janus colloid at various polar angles θ . The metal side corresponds to $0 \leq \theta < 90^\circ$, whereas the silica side corresponds to $90^\circ < \theta \leq 180^\circ$. For each θ , the ion concentration is averaged over $[\theta - 1.5^\circ, \theta + 1.5^\circ]$. The dashed horizontal line marks the bulk concentration. Due to the induced polarization charges, the ions aggregate around the metal hemisphere and are depleted on the silica side.

Although the dielectric effects are stronger for the silica/metal Janus colloid, $c(r, \theta)$ is still independent of θ for angles belonging to the same hemisphere. Thus, to a good approximation, one could use the angular average of the distribution over each hemisphere to characterize the system. Since the silica/silicon Janus colloid closely resembles an isotropic dielectric colloid, which has been well studied,⁵ from now on we focus on the silica/metal Janus colloid.

3.1.2 Asymmetric salt. Asymmetric 2 : 1 and 3 : 1 salts, such as MgCl_2 and AlCl_3 , are widely used in chemical systems. As noted above, multivalent ions experience quadratically stronger dielectric repulsion and attraction than monovalent ions, giving rise to a symmetry breaking near interfaces where a jump occurs in the relative permittivity. Fig. 6a and b illustrate this for the spatially varying ion concentration of a 2 : 1 salt (bulk concentration 50 mM) around a silica/metal Janus particle. The divalent cations (Fig. 6a) are strongly concentrated at the metal side while depleted at the silica side. However, for the monovalent anions (Fig. 6b), which have a four times smaller image potential energy, this imbalance is much weaker. Thus, although in the bulk the cation concentration C_{2+} is obviously half of the anion concentration C_{1-} , close to the silica hemisphere we

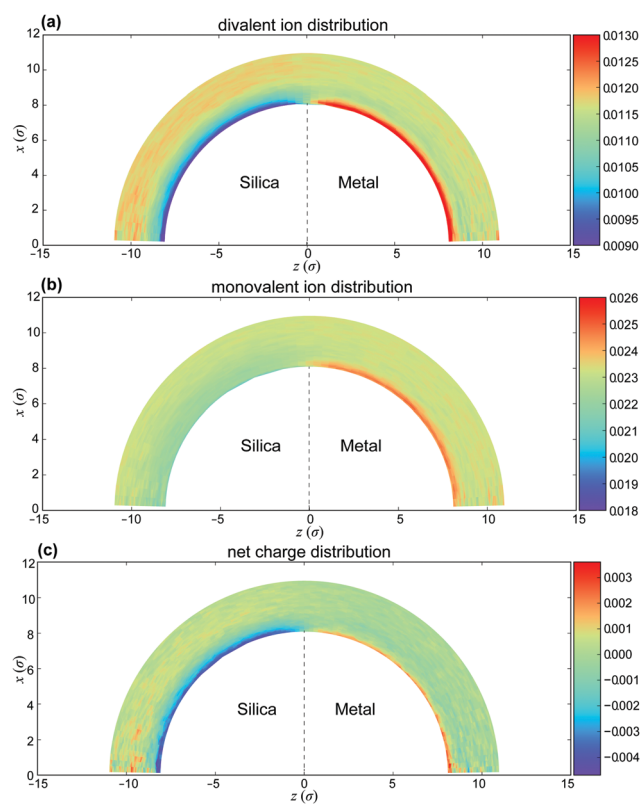


Fig. 6 Ion number density (σ^{-3}) distribution of a 2 : 1 electrolyte around an isolated silica/metal Janus colloid. The bulk concentration of 50 mM corresponds to $0.0110\sigma^{-3}$ for divalent ions and $0.0220\sigma^{-3}$ for monovalent ions. (a) Divalent cation density distribution, enhanced near the metal surface and suppressed near the silica surface; (b) monovalent anion density distribution, with significantly lower enhancement and suppression; (c) net ionic charge density distribution, negative near the silica hemisphere and positive near the metal hemisphere.

find $C_{2+}/C_{1-} < \frac{1}{2}$, resulting in a net negative ionic charge density (Fig. 6c). Similarly, a positive ionic charge density is observed at the metal side. This net ionic charge density close to the colloidal surface decreases near the transition between the two hemispheres ($z = 0$).

Although the net charge of the ion layers near the two hemispheres is opposite in sign, we anticipate that the difference in permittivity of the hemispheres causes both layers to induce negative polarization charges. This is confirmed in Fig. 7a, where both the metal surface and the silica surface are negatively charged but with different surface charge density. However, the net induced charge on the colloid must vanish, and accordingly we observe a ring of positive charges at the equator of the Janus particle, where three domains of different relative permittivity meet. A consequence of the polarization charge distribution on the colloid is that the particle and its associated ion cloud studied in Fig. 6 acquire an effective dipole moment when immersed in an asymmetric electrolyte.

Another interesting observation is that the fluctuations in the induced charges are rather different for the two hemispheres (Fig. 7b). This can be attributed to the fact that ions

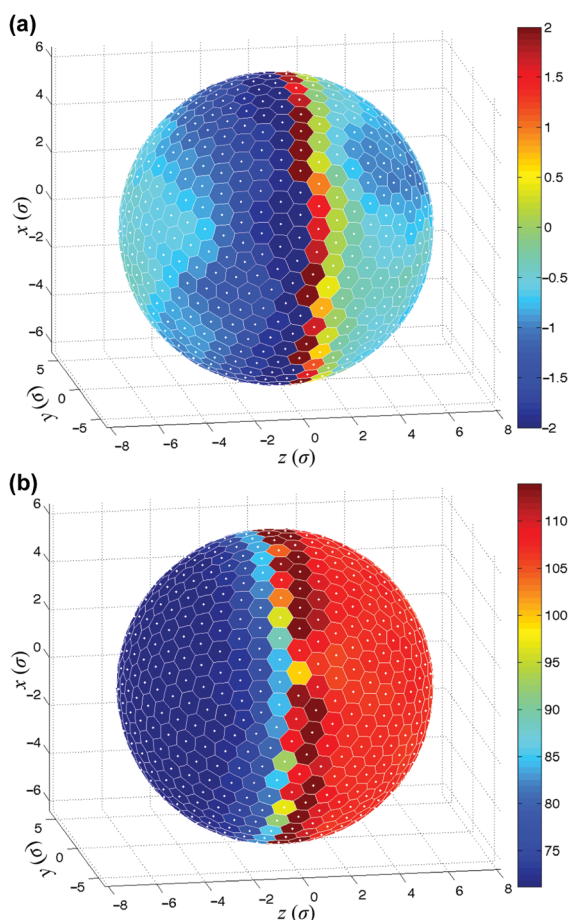


Fig. 7 (a) Net polarization charge density and (b) its standard deviation induced on a single silica/metal Janus colloid by 50 mM 2:1 electrolyte. Both the magnitude and the standard deviation are in units $10^{-5}e/\sigma^2$. Note how the fluctuations by far exceed the magnitude of the induced charge.

are more likely to interact with the dielectrically attractive metal hemisphere than with the repulsive silica hemisphere.

3.2 Counterion distribution near a charged dielectric Janus colloid

The situation changes when the Janus colloid also carries a free surface charge. Then, it will attract counterions from the solution that will form an electric double layer at the spherical surface. These ions interact with their induced charges on the Janus colloid as well as with the surface free charges. We are particularly interested in a strength comparison between the dielectric interactions and the intrinsic free-charge interactions.

3.2.1 Uniformly charged Janus colloid. We first consider an isotropically charged silica/metal Janus colloid of $Z = -60$ (-30.6 mC m^{-2}) surrounded by counterions (monovalent, $z = 1$, or divalent, $z = 2$) only. Fig. 8a shows the monovalent counterion density distribution. Although, just as for the silica/metal Janus particle in Fig. 6, dielectric effects attract the counterions to the metal side and repel them from the silica side, the attraction between the counterions and the surface free charges is so strong that it overwhelms the dielectric effects, resulting in little contrast between the two hemispheres. However, for divalent counterions the dielectric effects are sufficiently strong to produce a noticeable difference between the two hemispheres (Fig. 8b). This observation is consistent with a quick estimation of the interaction energies. The potential energy of a z -valent ion interacting with the free charge on the Janus colloid is $\frac{zZl_B}{r}k_B T = -7.5zk_B T$, where we have set $r = 8\sigma$ at contact and $l_B = \sigma$. The absolute interaction energy of such an ion with its

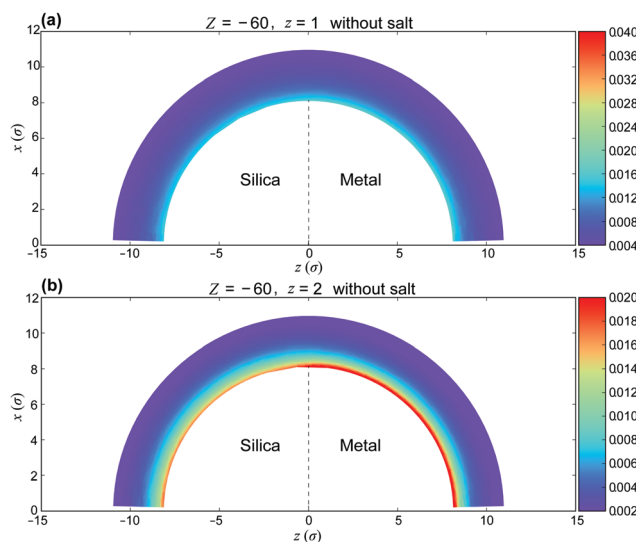


Fig. 8 Counterion distribution around a uniformly charged ($Z = -60$) dielectric silica/metal Janus colloid. The concentration is expressed as the number density (units of σ^{-3}) and no additional salt is present. For monovalent counterions (a), there is no discernible difference in the concentration between the two hemispheres, as the free surface charge overwhelms the dielectric effects. However, for divalent counterions (b) these effects are far stronger and the distribution becomes asymmetric. See main text for a quantitative discussion.

induced polarization charge is $|E_p| < \frac{|\Delta\epsilon|}{\epsilon} \frac{z^2 l_B}{2(r-7\sigma)} k_B T \approx \frac{1}{2} z^2 k_B T$, where the upper limit corresponds to a planar geometry and $\frac{|\Delta\epsilon|}{\epsilon} \approx 1$ for both hemispheres, but opposite in sign. Thus, for monovalent counterions the difference in image potential energy between the silica and metal hemispheres is approximately $2|E_p| \approx k_B T$ and the total attraction experienced by the ions (including the effect of free charge) is quite similar. However, for divalent counterions the difference in image potential energy is approximately $4k_B T$, as borne out by Fig. 8b.

Generally, the addition of salt is expected to diminish dielectric effects. To examine this, we also study the system with 20 mM and with 50 mM additional monovalent salt. These salt concentrations correspond to Debye lengths of 21.5 Å (3.01σ) and 13.6 Å (1.90σ), respectively. Here we focus on the divalent counterion system. As illustrated in Fig. 9, compared to a salt-free environment, the divalent counterions become less concentrated near the colloidal surface with increasing salt concentration. This weakened binding simply reflects the screening of the surface charge by the salt. However, the location of the maximum in the counterion density is almost independent of the salt concentration, as it is determined by short-range excluded-volume effects. Moreover, taking the ratio of the peak heights for the metal and the silica hemispheres as a measure of the dielectric effects, we observe that this ratio is essentially constant at 1.4 for the three salt concentrations—showing that the relative effects of the dielectric mismatch are not diminished by salt at the concentrations examined here. In fact, this ratio is directly related to the binding energy difference for divalent ions

between the metal and the silica hemispheres. Based upon our previous estimation, the interaction energy between a divalent ion and the free charge on the Janus colloid at contact is $-15k_B T$, while the image potential energy is $\pm 2k_B T$ on the silica and the metal side, respectively, which gives an energy ratio of $17/13 \approx 1.31$.

3.2.2 Anisotropically charged Janus colloid. In reality, a mismatch in dielectric properties typically implies a difference in surface chemistry as well, and the free-charge distribution on the surface of a Janus colloid may be anisotropic. For example, in water a silica surface will be negatively charged due to ionization,³⁵ whereas a metal surface would generally be minimally charged. Here, we examine how this additional anisotropy affects the equilibrium structure of the EDL. We consider a silica/metal Janus colloid immersed in a 20 mM 1:1 electrolyte. The typical surface charge density of an ionized silica particle is $\mathcal{O}(1)$ mC m⁻² in aqueous solutions with a pH spanning from 4 to 8 and with electrolyte concentrations ranging from 5 mM to 0.3 M.³⁶ Accordingly, we set the total free surface charge on the silica side to $2e^-$ or $10e^-$ (-2.04 mC m⁻² or -10.2 mC m⁻², respectively), while keeping the metal side neutral. Since the ionization of silica is an equilibrium process in which silanol groups that are randomly distributed over the surface dynamically dissociate and reassociate, we spread the free surface charge uniformly across the silica hemisphere to represent the thermal average. All the counterions in this system are monovalent.

For surface charge density -2.04 mC m⁻² on the silica hemisphere (triangular symbols in Fig. 10), the repulsive dielectric effects at the silica surface overwhelm the attraction from its surface free charge, leaving a weakly depleted region of counterions on the silica side. At the same time, the dielectrically attractive metal side exhibits an accumulation of counterions. Thus, apart from the difference in global salt concentration, this distribution essentially mimics the one in Fig. 5 (Section 3.1.1). This demonstrates that the EDL can be strongly altered by dielectric effects for realistic ionization states. However, when we increase the silica surface charge density to -10.2 mC m⁻² (circular symbols in Fig. 10), this hemisphere shows strong counterion accumulation, significantly surpassing the metal side. In fact, compared to the case with lower surface charge density, even the metal side exhibits a slight enhancement in the counterion density. This is due to the attraction from the negative free charges on the opposing (silica side) as well as the negative charges they induce on the metal surface.

3.3 Size effects

3.3.1 Colloidal size effects. Although the Janus colloid modeled in this paper is larger than in earlier simulations of dielectrically isotropic spheres,³⁷ it is still at least an order of magnitude smaller than particles used in most experiments. To verify that our findings apply to realistic particles, we revisit the divalent counterion distribution case of Section 3.2.1 with 20 mM 1:1 salt, and consider a Janus colloid with the same surface charge density as before, but four times larger diameter. To maintain the discretization accuracy in the IDS, the number of surface patches is increased by a factor 16.

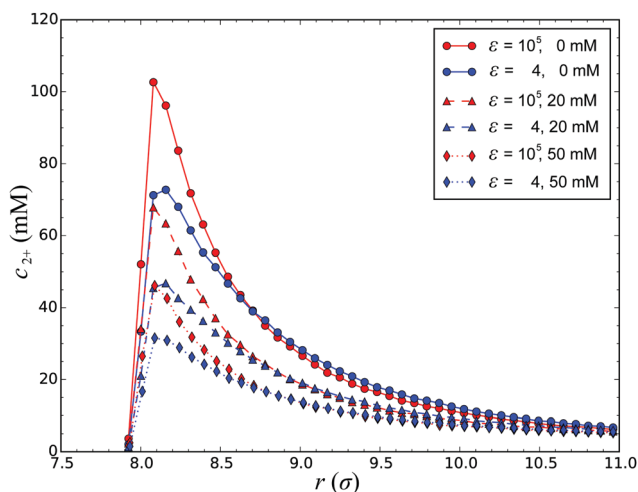


Fig. 9 Effect of salt on the density distribution of divalent counterions around a uniformly charged ($Z = -60$) silica/metal Janus colloid. Data are angularly averaged for each hemisphere (red: metal, blue: silica). As the concentration of 1:1 salt increases from salt free (circles, solid lines), to 20 mM (triangles, dashed lines) to 50 mM (diamonds, dotted lines), the colloid charge becomes increasingly screened and the accumulation of the counterions decreases. However, the effect of the dielectric mismatch between both hemispheres remains, with a near-constant ratio between the peaks in the concentrations around the metal hemisphere and the silica hemisphere.

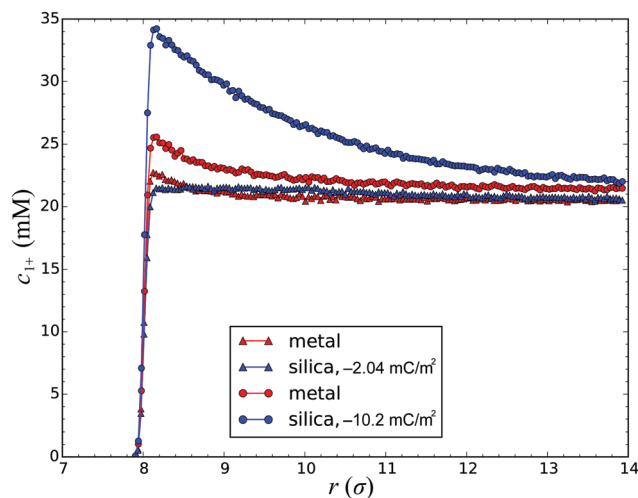


Fig. 10 Effect of anisotropic surface charge on the density distribution of monovalent counterions. The silica/metal Janus colloid is immersed in a 20 mM 1:1 electrolyte. The metal hemisphere carries no free charge (although it can acquire a polarization charge), whereas the silica hemisphere carries a uniform free surface charge density of either $2e^-$ (triangles) or $10e^-$ (circles). Curves show the concentration of positive ions around either hemisphere, angularly averaged. For low free charge density on the silica surface, the attractive polarization charge (induced by ions) on the metal side dominates, but once the surface charge on the silica hemisphere is increased, the electric double layer becomes concentrated on that side. Interestingly, even the ion concentration on the metal side is slightly increased by the free charges on the silica hemisphere. For consistency, we note that the enhancement of positive ions around both hemispheres above the bulk concentration is quantitatively consistent with the number of excess counterions present.

Moreover, to permit extrapolation to even larger particles, we also model planar metallic and silica interfaces with the same surface charge density, which correspond to an infinitely large Janus colloid. As shown in Fig. 11, with increasing colloidal size the divalent ions become more concentrated at the surface. This is mainly due to stronger attraction exerted by the free surface charge and can be understood from a simple analysis. Consider a z -valent ion at a distance Δx from a uniformly charged Janus particle radius R_d (referring to the location of dielectric jump, solid circle in Fig. 1), and free surface charge density σ_f . The electrostatic force exerted by the surface free charges then can be written as $(4\pi\sigma_f z l_B k_B T/e) \left(\frac{R_d}{R_d + \Delta x}\right)^2$ and, for fixed Δx , increases with R_d . On the other hand, the force also decays with ion distance Δx , at a rate that decreases with increasing colloid size—reaching a constant value in the planar limit. As a result, more ions are concentrated close to the surface when the colloid size increases. Despite this variation of density profile with colloid size (represented by the trends in Fig. 11), the contrast between the metal and silica hemispheres persists. Indeed, if we consider the maximum density ratio between the two hemispheres, the four times larger Janus colloid still gives the same ratio 1.4 ratio as in Section 3.2.1. For the planar limit, the ratio reduces to 1.307, coinciding with the ratio 17/13 predicted in our previous energy analysis.

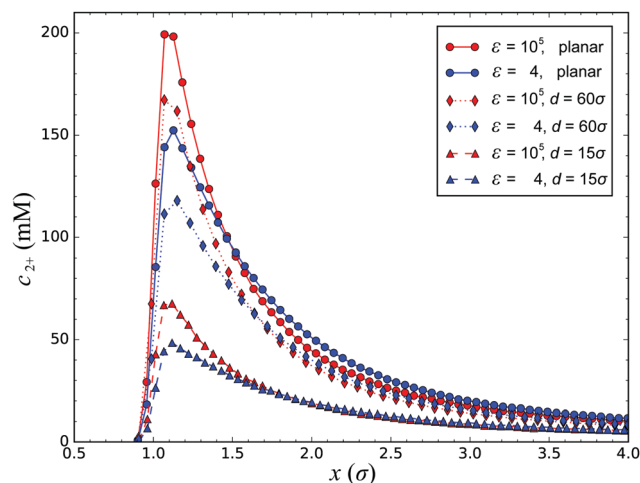


Fig. 11 Effect of colloidal size on the density distribution of divalent counterions immersed in 20 mM 1:1 salt. The silica/metal Janus colloids are uniformly charged with surface free charge density $\sigma_f = -9.74 \times 10^{-2} e/\sigma^2$. The density profiles are shifted such that the horizontal axis represents the distance x of the ions to the dielectric interfaces. As the Janus colloid diameter increases from 15σ (triangles and dashed lines; data of Fig. 9) to 60σ (diamonds and dotted lines) and to infinity (circles and solid lines; planar interface), the counterions are more attracted to the surface, but the contrast in the counterion distribution between the metal and the silica hemispheres persists.

3.3.2 Ionic size effects. Until this point, we have employed a constant ion size. However, the hydrated ion radius typically increases with valence,³⁸ which would affect both the excluded-volume interactions and the electrostatic binding in our simulations. To assess the magnitude of these effects, we revisit the system of Section 3.1.2, *i.e.*, a neutral silica/metal Janus colloid immersed in 50 mM 2:1 electrolyte, except that the divalent ions are 20% larger. As shown in Fig. 12, the concentration of

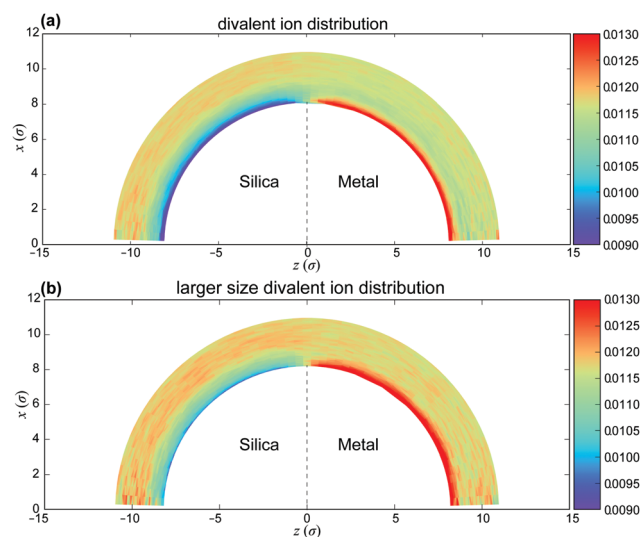


Fig. 12 Divalent ion number density (σ^{-3}) distribution of 50 mM 2:1 electrolyte around a silica/metal Janus colloid. (a) Both monovalent and divalent ions have diameter σ ; same data as in Fig. 6(a); (b) the same system, but with divalent ions of diameter 1.2σ .

divalent ions near the surface is systematically higher for the simulations with larger sizes (panel b). If we angularly average the density profile for each hemisphere (data not shown), we find that for both ion sizes the ion distributions approach the bulk density at very similar distances from the colloidal surface. Since the larger ions cannot approach the colloidal surface as closely as the smaller ones, the thickness of the electric double layer is effectively reduced, and the ion concentration is increased accordingly. In principle, this change in the distribution of the divalent ions could in turn affect the density profiles of the (unaltered) monovalent ions as well as the induced surface charge densities, but no statistically significant differences are observed.

4 Summary

We have presented a systematic examination of dielectric effects on the ion distribution around a spherical Janus particle embedded in an aqueous electrolyte solution. We have employed molecular dynamics simulations supplemented with a boundary-element-based preconditioned dielectric solver that computes induced polarization charges at each time step, at all dielectric interfaces.^{26,28} Via finite-element calculations we demonstrated that Janus particles created by metallic coatings can—as far as dielectric effects are concerned—be accurately represented as composed of two evenly divided hemispheres with a dielectric mismatch at the equatorial interface.

We have investigated two typical Janus particles that are representative in their dielectric configurations, namely silica/silicon and silica/metal. If such a colloid is neutral, ions are depleted from (or attracted to) the silica (or metal) hemispheres due to the dielectric contrast with the surrounding medium. Whereas a silica/silicon Janus colloid behaves effectively similar to a dielectrically isotropic particle, a silica/metal Janus colloid shows clear anisotropy in the surrounding ion distribution. In an asymmetric electrolyte, dielectric effects can even result in the generation of an effective electric dipole moment on the colloid.

For uniform highly charged silica/metal Janus colloids, the EDL contrast persists even at high salt concentration, especially for divalent counterions. As a more realistic model, we have also considered an anisotropically charged silica/metal Janus colloid. We found that dielectric effects still suppress the counterion concentration on the silica side, unless this hemisphere is highly ionized. These results demonstrate that dielectric effects cannot be ignored for the EDL structure of Janus particles.

Dielectric effects, even with the efficient solver of ref. 26 and the preconditioning techniques of ref. 28, are computationally costly. As a result, the Janus colloids are modeled here as significantly smaller than their typical experimental counterparts. However, as demonstrated in Section 3.3, the analysis presented remains applicable for larger particles. Although free charge interactions may vary, the dielectric effects are hardly affected.

Our findings not only clarify the effect of dielectric mismatch on the electrolyte distribution around synthetic Janus colloids, which is crucial for their colloidal interfacial properties, but also offer a

potential avenue to control dielectric self-assembly²⁷ and may have implications for biological entities with dielectric anisotropy.

Acknowledgements

This research was supported through award 70NANB14H012 from the U.S. Department of Commerce, National Institute of Standards and Technology, as part of the Center for Hierarchical Materials Design (CHiMaD), the National Science Foundation through Grant No. DMR-1121262 at the Materials Research Center of Northwestern University and DMR-1310211, and the Center for Computation and Theory of Soft Materials (CCTSM) at Northwestern University. We thank the Quest high-performance computing facility at Northwestern University for computational resources.

References

- 1 Y. Levin, *Rep. Prog. Phys.*, 2002, **65**, 1577–1632.
- 2 A. Stradner, H. Sedgwick, F. Cardinaux, W. C. K. Poon, S. U. Egelhaaf and P. Schurtenberger, *Nature*, 2004, **432**, 492–495.
- 3 P. Linse and V. Lobaskin, *Phys. Rev. Lett.*, 1999, **83**, 4208–4211.
- 4 H. Morgan and N. G. Green, *AC electrokinetics: colloids and nanoparticles*, Research Studies Press, Baldock, UK, 2003.
- 5 R. Messina, *J. Chem. Phys.*, 2002, **117**, 11062–11074.
- 6 A. P. dos Santos, A. Bakhshandeh and Y. Levin, *J. Chem. Phys.*, 2011, **135**, 044124.
- 7 L. Lue and P. Linse, *J. Chem. Phys.*, 2011, **135**, 224508.
- 8 Z. Gan, X. Xing and Z. Xu, *J. Chem. Phys.*, 2012, **137**, 034708.
- 9 R. O. James and G. A. Parks, in *Surface and Colloid Science*, ed. E. Matijević, Plenum, New York, 1982, vol. 12, ch. 2, pp. 119–216.
- 10 A. B. Pawar and I. Kretzschmar, *Macromol. Rapid Commun.*, 2010, **31**, 150–168.
- 11 S. Jiang, Q. Chen, M. Tripathy, E. Luijten, K. S. Schweizer and S. Granick, *Adv. Mater.*, 2010, **22**, 1060–1071.
- 12 A. Walther and A. H. E. Müller, *Chem. Rev.*, 2013, **113**, 5194–5261.
- 13 J. Zhang, E. Luijten and S. Granick, *Annu. Rev. Phys. Chem.*, 2015, **66**, 581–600.
- 14 T. Nisisako, T. Torii, T. Takahashi and Y. Takizawa, *Adv. Mater.*, 2006, **18**, 1152–1156.
- 15 L. Hong, A. Cacciuto, E. Luijten and S. Granick, *Nano Lett.*, 2006, **6**, 2510–2514.
- 16 Q. Chen, J. K. Whitmer, S. Jiang, S. C. Bae, E. Luijten and S. Granick, *Science*, 2011, **331**, 199–202.
- 17 S. Jiang, J. Yan, J. K. Whitmer, S. M. Anthony, E. Luijten and S. Granick, *Phys. Rev. Lett.*, 2014, **112**, 218301.
- 18 J. Yan, M. Bloom, S. C. Bae, E. Luijten and S. Granick, *Nature*, 2012, **491**, 578–581.
- 19 S. K. Smoukov, S. Gangwal, M. Marquez and O. D. Velev, *Soft Matter*, 2009, **5**, 1285–1292.
- 20 S. Gangwal, O. J. Cayre, M. Z. Bazant and O. D. Velev, *Phys. Rev. Lett.*, 2008, **100**, 058302.

- 21 M. C. Hagy and R. Hernandez, *J. Chem. Phys.*, 2012, **137**, 044505.
- 22 M. M. Moghani and B. Khomami, *Soft Matter*, 2013, **9**, 4815–4821.
- 23 S. J. de Carvalho, R. Metzler and A. G. Cherstvy, *Phys. Chem. Chem. Phys.*, 2014, **16**, 15539–15550.
- 24 S. Gangwal, O. J. Cayre and O. D. Velev, *Langmuir*, 2008, **24**, 13312–13320.
- 25 Z. Gan, H. Wu, K. Barros, Z. Xu and E. Luijten, *J. Comput. Phys.*, 2015, **291**, 317–333.
- 26 K. Barros, D. Sinkovits and E. Luijten, *J. Chem. Phys.*, 2014, **140**, 064903.
- 27 K. Barros and E. Luijten, *Phys. Rev. Lett.*, 2014, **113**, 017801.
- 28 H. Wu and E. Luijten, *Accurate and efficient numerical simulation of dielectrically anisotropic particles*, 2016, submitted.
- 29 M. Han, H. Wu and E. Luijten, *Eur. Phys. J.: Spec. Top.*, 2016, **225**, 685–698.
- 30 Y. Saad and M. H. Schultz, *SIAM J. Sci. Stat. Comput.*, 1986, **7**, 856–869.
- 31 R. Wang and Z.-G. Wang, *Phys. Rev. Lett.*, 2014, **112**, 136101.
- 32 F. Fahrenberger, O. A. Hickey, J. Smiatek and C. Holm, *Phys. Rev. Lett.*, 2015, **115**, 118301.
- 33 R. W. Hockney and J. W. Eastwood, *Computer Simulation Using Particles*, McGraw-Hill, New York, 1981.
- 34 E. L. Pollock and J. Glosli, *Comput. Phys. Commun.*, 1996, **95**, 93–110.
- 35 S. H. Behrens and D. G. Grier, *J. Chem. Phys.*, 2001, **115**, 6716–6721.
- 36 J. Sonnefeld, A. Göbel and W. Vogelsberger, *J. Colloid Polym. Sci.*, 1995, **273**, 932–938.
- 37 R. Messina, E. González-Tovar, M. Lozada-Cassou and C. Holm, *Europhys. Lett.*, 2002, **60**, 383–389.
- 38 J. N. Israelachvili, *Intermolecular and Surface Forces*, Academic, San Diego, 3rd edn, 2011.